The Fengyun-4B Digital Fluxgate Magnetometer

Cheng-Han Weng[1,2]†, Bin Zhou[1,2]†, Yong-Liang Xue[1,2], Yu-Qi Tong[1,2,3], Bing-Jun Cheng[1,2], Yi-Teng Zhang[1,2], Jin-Dong Wang[1,2], Lei LI[1,2] *, Xin Zhang[4], Ru-Yi Zhang[5], Li-Guo Zhang[5], Jian-Guang Guo[6,7], Wei-guo Zong[6,7], Bo Chen[6,7], Xiao-Xin Zhang[6,7] *, Jin-song Wang[6,7]

1. State Key Laboratory of Space Weather, National Space Science Center, Chinese Academy of Sciences, Beijing, China

2. Key Laboratory of Solar Activity and Space Weather, National Space Science Center, Chinese Academy of Sciences, Beijing, China

3. School of Astronomy and Space Science, University of Chinese Academy of Sciences, Beijing, China

4. Beijing Key Laboratory of Space Environment Exploration, National Space Science Center, Chinese Academy of Sciences, Beijing, China

5. Shanghai Institute of Satellite Engineering, Shanghai, China

6. Key Laboratory of Space Weather, National Satellite Meteorological Center (National Center for Space Weather), China Meteorological Administration, Beijing, China

7. Innovation Center for FengYun Meteorological Satellite (FYSIC), China Meteorological Administration, Beijing, China

*Corresponding author: Lei LI (lil@nssc.ac.cn) ; Xiao-Xin ZHANG (xxzhang@ cma.gov.cn).

†Cheng-han Weng and Bin Zhou are co-first authors of the article

Key Points:

- The FY-4B magnetometer uses digital fluxgate technology with the Σ-Δ frame to realize digital quantization of magnetic field with high SNR.
- After ground calibration and in-orbit test, FY-4B FGM shows good performance in GEO orbital magnetic field monitoring
- The FY-4B magnetometer observations are comparable with the GOES-16 satellite, geomagnetic stations and magnetic field models.

Abstract

This paper describes the development of the fluxgate magnetometer on the Fengyun-4B satellite. The Fengyun-4 is the second generation of China's geostationary orbit satellite with the function of monitoring the space environment in GEO orbit. A fluxgate magnetometer (FGM) is deployed on this satellite to observe the magnetic field as a necessary input to space weather forecasting. This payload adopts three 3-axis fluxgate sensors to obtain space magnetic field data by excluding the satellite's interference. Each three-axis fluxgate sensor has an independent signal processing circuit. FGM uses digital signal processing technology to acquire magnetic field signals. First, the analog signal is oversampled using a high-speed ADC, then digital signal processing, such as phase-sensitive demodulation, integration, and filtering, is performed inside the FPGA, and the feedback signal is output to the feedback coil through the DAC. This signal processing loop constitutes an ADC system, and the quantization accuracy of the output digital quantity can reach 18 bits. the FGM performs in-orbit calibration during satellite rotation maneuver and Alfven wave events. Comparison with the GOES-16 satellite and Tsyganenko magnetic field model proves FGM to be effective in monitoring the magnetic field of the space environment. Through joint observations with GOES-16 satellite and geomagnetic stations, FY-4B describes the development of a typical magnetic storm on November 4, 2021. The Ground calibration and in-orbit preliminary results show the FY-4B satellite magnetometer outputs 20 bits of digital resolution data at a 30 Hz sampling rate, with the noise lower than $3\times10^{-4}nT^2/Hz@1Hz$ in the ±600nT range.

Plain Language Summary:

As a meteorological satellite, the Fengyun-4B can monitor almost the entire Eastern Hemisphere from the geostationary orbit, including the Earth's environment, and the space environment around the Earth as well. The magnetic field observation is one of the tasks. The magnetic field instrument adopts a new design, the signals of the sensors are digitized and processed by software in the processor. This approach can enhance the instrument performance and reduce the size of the instrument. This article describes the ground tests of the magnetometer. Through these tests, the instrument's performance is fully evaluated, key parameters are calibrated, the instrument is prepared for space observation. Now the magnetometer is operating in the geosynchronous orbit. After comparing with the GOES-16 satellite and the magnetospheric magnetic field model, we concluded that the Fengyun-4B magnetometer is working well in orbit. During a solar storm, Fengyun-4B observed the onset, main phase and recovery of the storm, allowing us to gain a deep understanding of the magnetic storm.

1 Introduction

The Fengyun-4 (FY-4) is the second generation of Chinese geosynchronous orbit meteorological satellite. The FY-4A and FY-4B satellites were successfully launched in Xichang, China, in December 2016 and June 2021, respectively. The FY-4 satellites are deployed with space environment monitoring instrument packages to detect parameters of the space environment such as magnetic fields, energetic particles, and radiation effects (Yang et al., 2017). Among them, the magnetometer of the FY-4 satellite inherited the fluxgate magnetometer technology from the YingHuo-1 fluxgate magnetometer (Zhou et al., 2009), which was also successfully applied to the HPM of the CSES mission launched in February 2018 (Cheng et al., 2018). The magnetometer signal of the FY-4A satellite is processed according to the traditional analog

signal processing method; while the FY-4B satellite magnetometer adopts the digital signal processing technique.
Fluxgate digital signal processing techniques have been being developed rapidly in recent years and widely used in space exploration. For example, digital fluxgate magnetometer technology is used in space missions such as Astrid-2 (Erik et al., 1999), Venus Express (Zhang et al., 2007), and BepiColombo (Glassmeier et al., 2010), where the input and output of analog signals are realized using ADC and DAC, and the processing of signal demodulation is performed inside the FPGA (Baumjohann et al., 2010). This technique has advantages over analog signal processing techniques, in reducing the number of chips, and improving the radiation hardness. However, its disadvantages are also obvious, the limited quantization accuracy of the DAC affects the resolution and linearity of the instrument. The use of oversampling and sigma-delta technology can improve the overall data quantization accuracy. In general, the overall magnetometer data quantization bits can be increased by 2 to 4 bits compared to the DAC quantization bits. This digital signal processing technology is currently mainly used in low magnetic field measurement. In the GEO orbit where FY-4B operates, the magnetic field is generally within 200nT, which is ideal for the application of digital fluxgate technology.
In this paper, the design and calibration of the digital fluxgate magnetometer (FGM) for the FY-4B satellite will be presented in the following sections, respectively.

2 Instrument Requirements

Magnetic field detection in GEO enables the monitoring of the geomagnetic storms and substorms, studying the solar wind interaction with the magnetosphere. Continuous magnetic field observation for a long time is of great significance to the forecast of space weather and scientific research.
In GEO orbit, the magnetic field is usually around 100~200nT. During the geomagnetic activity, the magnetic field fluctuates considerably. Referring to the observation results of the GOES-16 satellite, and considering a certain design margin, the measurement range of FGM is required to be ±600nT. To better observe the abundant low-frequency plasma waves in the GEO orbit, the bandwidth of FGM is required to be between DC-7Hz, and the noise is $0.01nT/Hz^{1/2}$. According to the requirements of measurement range and noise, the SNR of the instrument needs to reach 100 dB. The digital signal processing scheme can achieve a balance among digital resolution, hardware resources, and reliability.

3 Instrument Description

The FY-4B FGM consists of three 3-axis fluxgate sensors. Each sensor owns a separate digital signal processing electronic board. Three electronic boards are mounted in an electronic box. Figure 1 shows a picture of the FY-4B FGM flight model. The interference from the satellite can be better evaluated by the three fluxgate sensors, and this redundant design also improves the overall reliability of the instrument.

Figure 1. The flight model of the FY-4B FGM includes three sensors and one electronic box.

The sensors are mounted on a 6 m boom as shown in Figure 2. The +X of the FGM is aligned with the -Y axis of the satellite, the +Y axis of the sensor is aligned with the -X axis of the satellite, and the +Z axis of the sensor is aligned with the -Z axis of the satellite. The +Z of the satellite points to the earth. From April to September, the +X of the satellite points to the direction of flight, and the +Y of the FGM points to the west; from October to following March, the satellite roll over around the Z axis, with -X pointing to the direction of flight and +Y of the FGM pointing to the east.

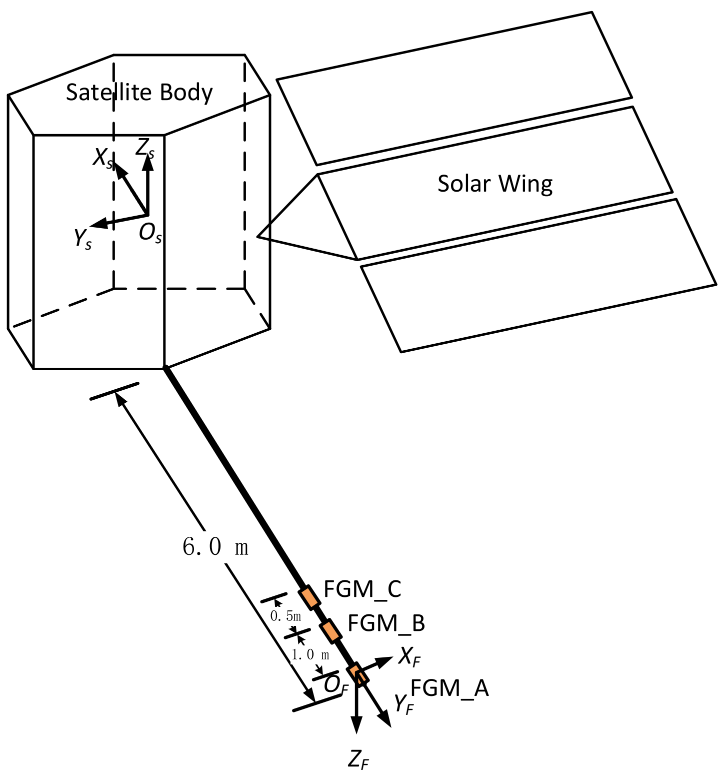

Figure 2. The FGM sensors on the boom of FY-4B. The $O_sX_sY_sZ_s$ is the FY-4B body coodiation, and the $O_FX_FY_FZ_F$ is the FGM sensor coodiation.

3.1 Sensor

Each single-axis fluxgate sensor is composed of three coils, including an excitation coil, a signal coil, and a feedback coil, see Figure 3(a), where the excitation coil is a spiral ring coil wrapped around a ring core made of high magnetic permeability material. The three single-axis sensors are mounted orthogonally to form a three-axis fluxgate sensor, and the internal structure of the sensor is shown in Figure 3(b). The magnetic field generated by the excitation current makes the core material magnetically saturated periodically. The signal coil has an annular magnetic flux inside, and the projection of the positive and negative magnetic flux in the axial direction of the signal coil is balanced. The superposition of the external magnetic field and the excitation field is constrained by the magnetic saturation of the core material, and the magnetic flux in the signal coil appears as a second harmonic signal at the excitation frequency, and the intensity of this signal is proportional to the external magnetic field.

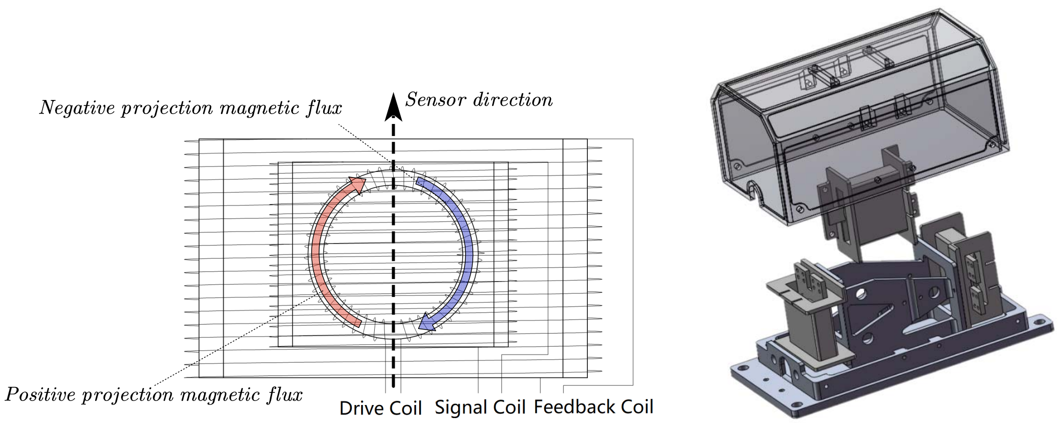

(a) (b)

Figure 3. The internal structure of the FGM sensor. (a) The structure of the fluxgate sensor and magnetic flux inside the ring core. (b) The orthogonal mounting layout of three-axis sensors.

3.2 Electronics

Normal fluxgate signal processing includes a pre-amplifier, phase-sensitive demodulator, integrator, filters, and V-I amplifier. Figure 4 shows a block diagram of the digital signal processing circuit of the FGM. In this case, only the pre-amplifier and V-I amplifier are hardware analog circuits. The pre-amplified signal is digitally sampled at high-speed through 12-bit ADC. In FPGA, phase-sensitive demodulation, integrator, and filtering will be realized by software. Finally, the digital signal is converted into a voltage signal through 14bit DA and output to the V-I amplifier. The FGM measurement has two ranges, ±600nT in orbit and ±65000nT for the ground test, which are realized by switching the feedback resistance. To make the magnetic field detection stable when the board temperature changes, resistance with a temperature drift coefficient of 5ppm is used as the feedback resistance.

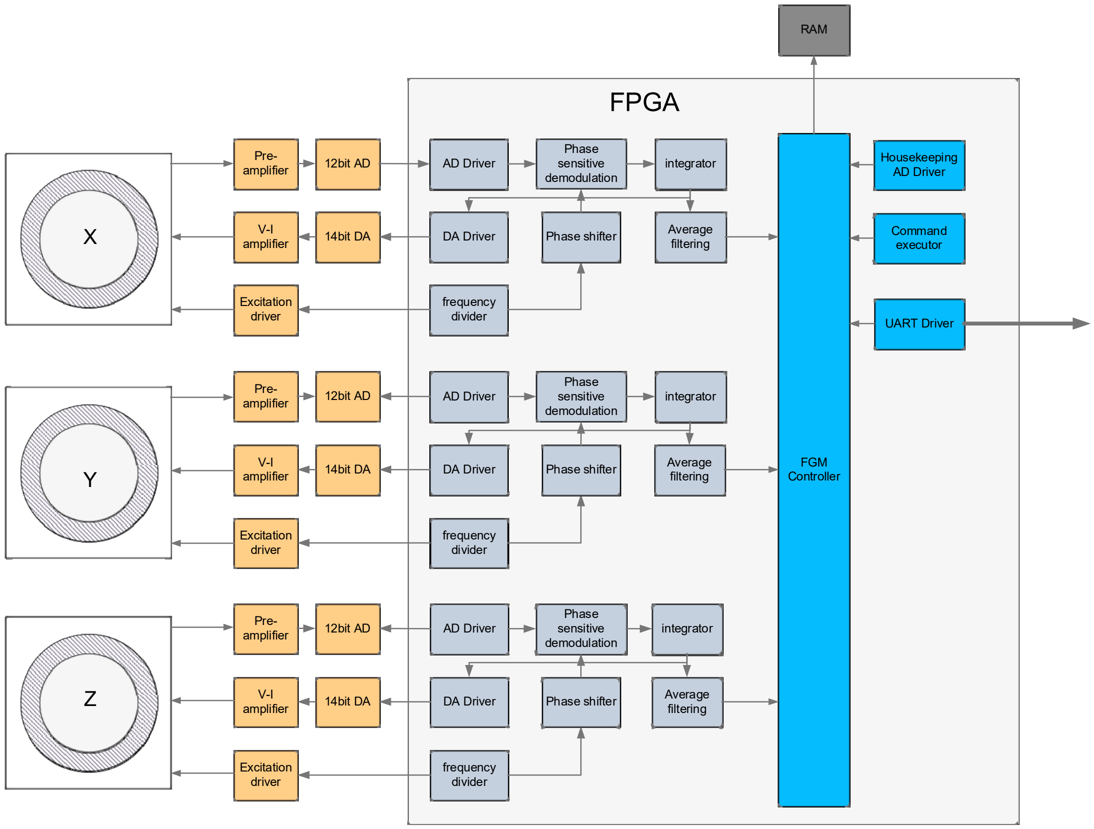

Figure 1. FGM circuit block diagram

3.3 Digital fluxgate signal processing of model

A digital fluxgate magnetometer is equivalent to an "ADC" device that converts a magnetic field into a digital value. Through modeling and simulation, the performance of the device can be confirmed, which is also the performance limit of the magnetometer. As far as possible, a real magnetometer signal can be modeled. When the excitation frequency is f0, the magnetic field is modulated by the sensor at 2f0. Since the excitation coil cannot be perfectly uniform, f0 and its odd harmonics are also induced by the signal coil. So f0 and 2f0 signals are used to simulate the sensor signal, as shown in Figure 5. The f0 signal does not contain magnetic field information, but its oscillation modulation of the 2f0 signal is beneficial to signal detection.

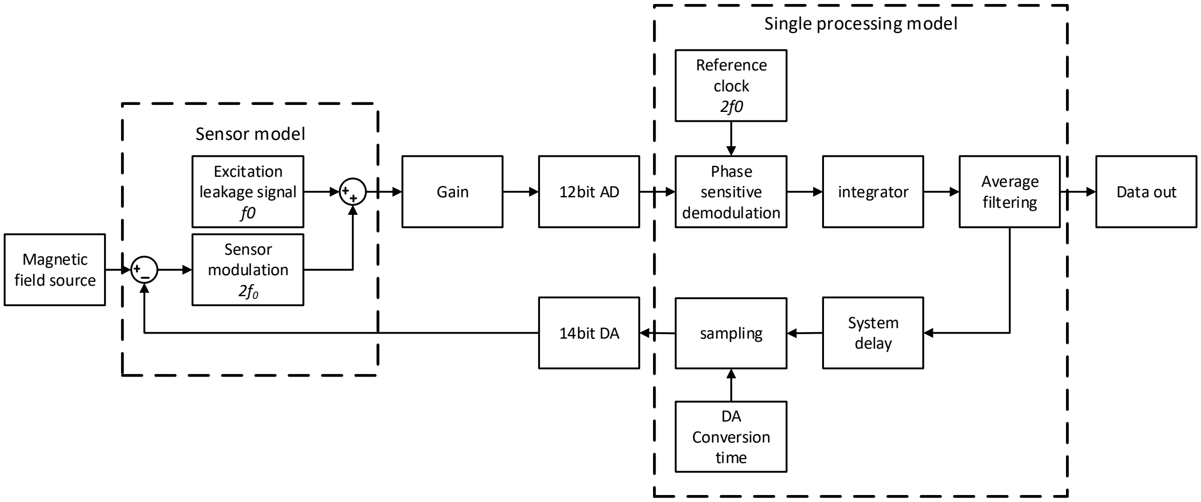

Figure 2. Simulation model of the fluxgate signal digital processing process

Figure 6 shows the simulated linear output of numerical processing. According to the output data of 20bit digital resolution, the maximum linear error is about 4 LSB, which is equivalent to a linear error of 5pT in a range of ±600nT. This linear error is negligible for the FY-4B magnetic field detection. Using this model, we further obtain the SNR of digital signal processing. Figure 7 shows the PSD of a sinusoidal signal with 600nT amplitude before it is filtered and 30Hz sampled after digital signal processing. According to the output data of 20bit digital resolution, the noise is lower than 1 LSB/√Hz, and the corresponding magnetic field noise is 1pT/√Hz. The RMS noise in the band is better than 5 LSB in an effective bandwidth of 15Hz, and the SNR is 106dB after 30Hz sampled. Considering the linearity of digital signal processing and noise simulation results, the effective digital resolution of FGM is 18-bit. Considering a certain margin in the design, the magnetic field data of FGM can reach a 20-bit resolution.

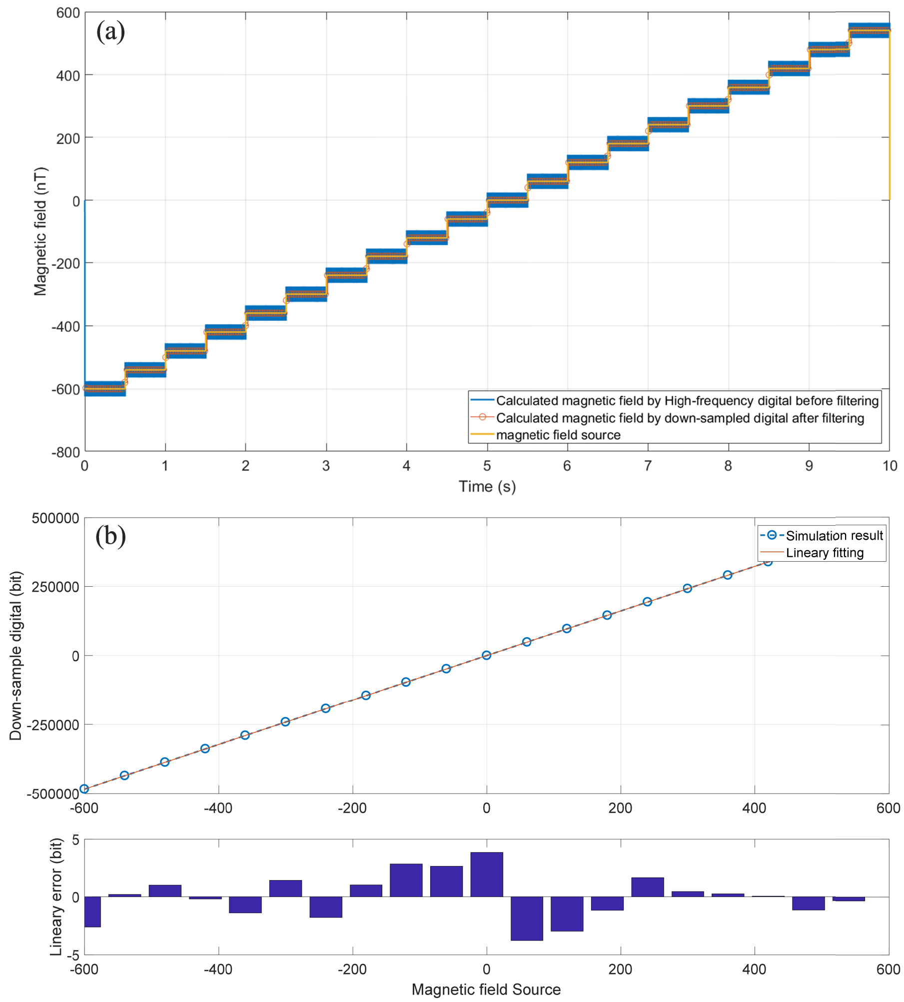

Figure 3. The simulated linearity of the digital magnetometer model

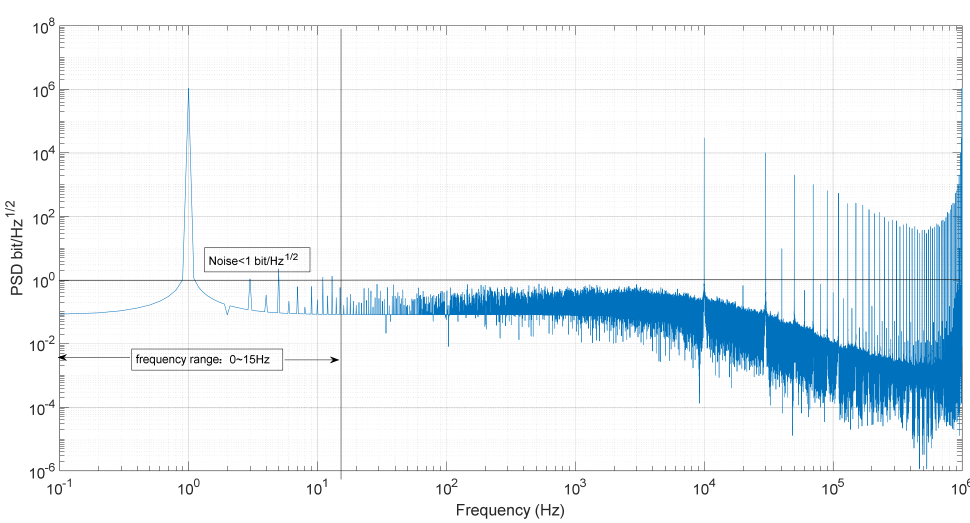

Figure 4. Noise performance of the digital magnetometer model

4 Calibration

4.1 Linearity test

The linearity test was carried out in a Helmholtz coil at the Fragrant Hills Weak Magnetic Laboratory, National Institute of Metrology, China, which is the Chinese magnetic field measurement benchmark. The Laboratory has been used to calibrate the magnetometer of Yinghua-1 (Zhou et al., 2009) and CSES (Zhou et al., 2018). The test needs a Special coil system (Figure 8(a)). Coil 1 compensates for the geomagnetic field in the XYZ direction, while coil 2 compensates for the geomagnetic field in the XY direction. The drift in the Z direction of the geomagnetic field is approximately equal to the scalar magnetic field in coil 2. The optic-pump magnetometer in coil 2 monitors this drift and compensates for the Z direction of coil 1. This ensures the stability of the standard magnetic field in the Z-direction. This method can make the magnetic field uncertainty no greater than 1nT.

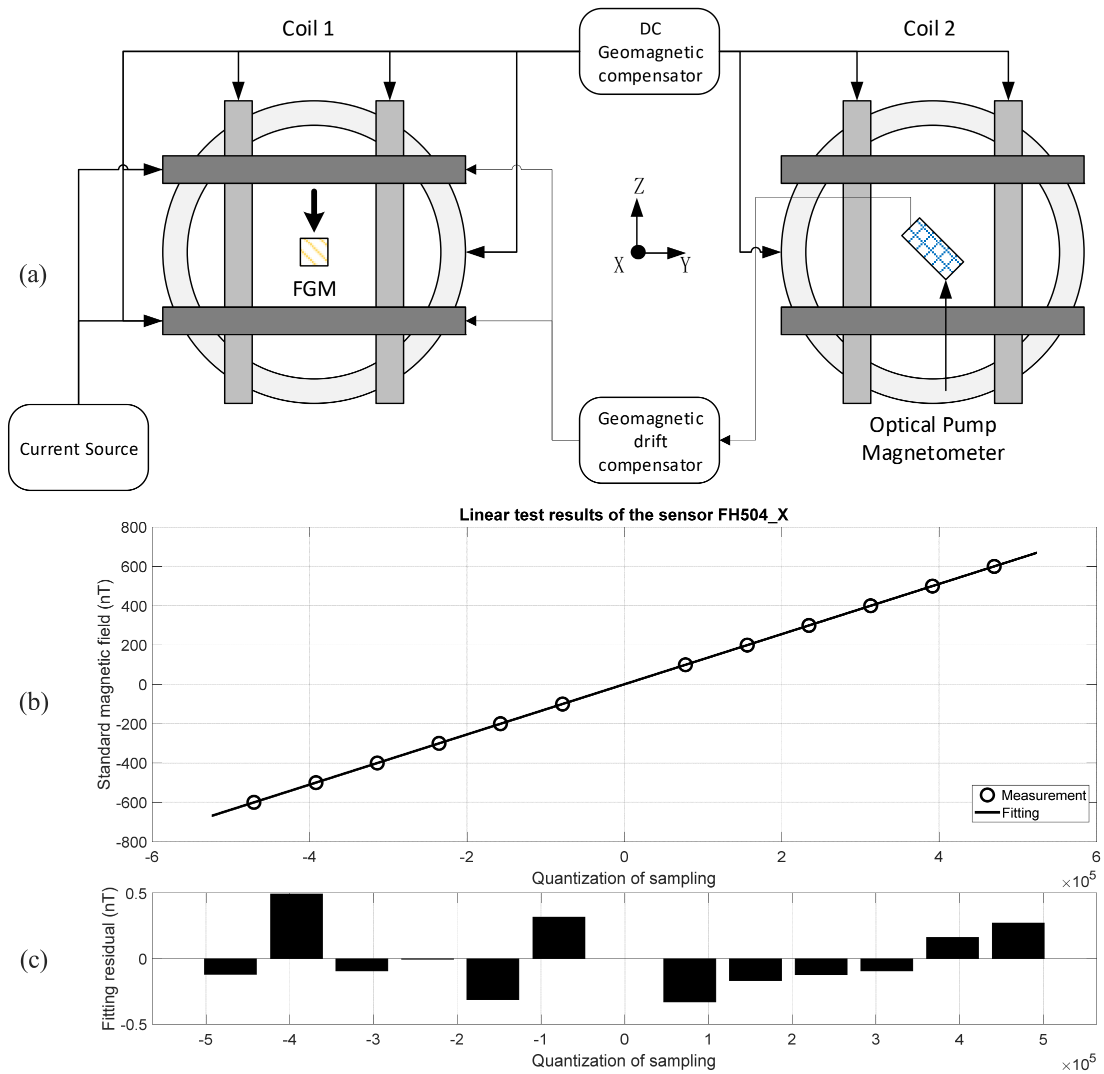

Figure 8. Coil system for linearity test and the test result. (a) The coil system for the linearity test consists of two triaxial Helmholtz coils, the main coil (left) is used to generate the standard magnetic field and the other coil (right) is used to monitor the drift of the geomagnetic field. (b)/(c) The maximum linear error is 0.5nT, which is within the uncertainty of the test system

The magnetic field in coil 1 can be calculated from the current and changed by the 100nT step. The relationship between the magnetic field and measurement of the FGM can be fitted as a straight line, and the ratio of fitting error to measurement range is the linearity of FGM. Figure 8(b) and (c) shows the linearity test result of the FGM A X-axis, and it reaches 0.038%.

4.2 Orthogonality test

In the orthogonality test, FGM works in the range of ±65000nT to improve the sensitivity to non-orthogonality. A magnetic field of 50000nT is applied to coil 1 used in the linearity test. The FGM sensor is rotating in the coil to measure the magnetic field of different relative directions.

The orthogonal coefficients of the sensor are calculated by scalar equation (Zhou et al., 2018). Figure 9 shows the coverage of the measured magnetic field vector on a sphere, and the orthogonality calibration greatly reduces the scalar difference of FGM at about 50000nT. The uncertainty in the orthogonality is less than 0.01°. In the range of 600nT, the projection error caused by the non-orthogonal angle variation would not exceed 1nT after correction.

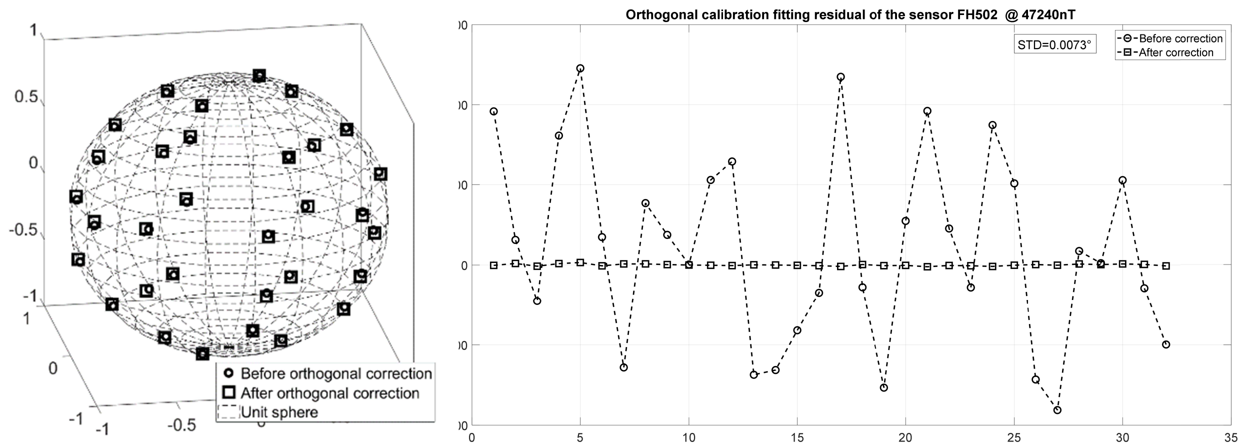

Figure 9. The angular distribution of the magnetic field in the Orthogonality test(left) and Comparison of scalar heading difference before and after orthogonality correction(right).

4.3 Frequency response test

This test was also performed in the Helmholtz coil, which is used to compensate for the geomagnetic field and generate AC magnetic field from 4Hz to 10Hz, and the FGM measurement is recorded at the same time. Figure 10 shows the signal amplitude response at these frequencies. The -3db bandwidth of each component of FGM is above 7Hz. In a digital magnetometer, the amplification factor of the magnetic field affects the frequency response. The signal amplitude of each axis sensor and the corresponding amplification are manually optimized. So, the frequency response of each component is not the same as can be seen from the test results.

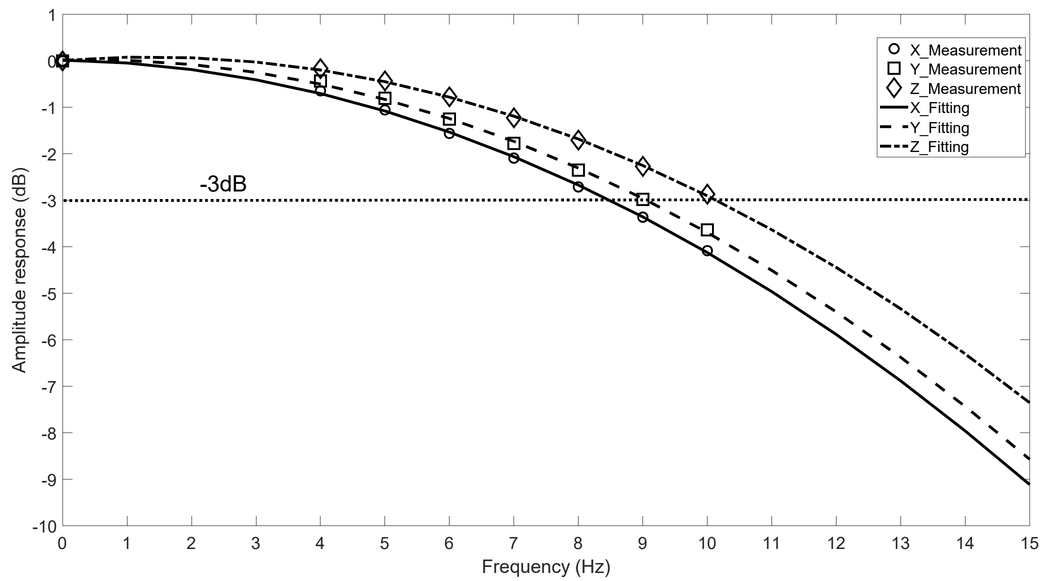

Figure 10. Frequency response of FGM A

4.4 Noise test

The noise test of FGM was carried out in a 600mm diameter and 2m length magnetic shield in the weak magnetism laboratory of the National Space Science Center, CAS. Inside the magnetic shield, the remanence can be less than 1 nT. It can effectively reduce external magnetic field disturbances. Figure 11 shows the PSD curve of the noise test. The PSD of noise is lower than that of $3\times10^{-4}nT^2/Hz$@1Hz

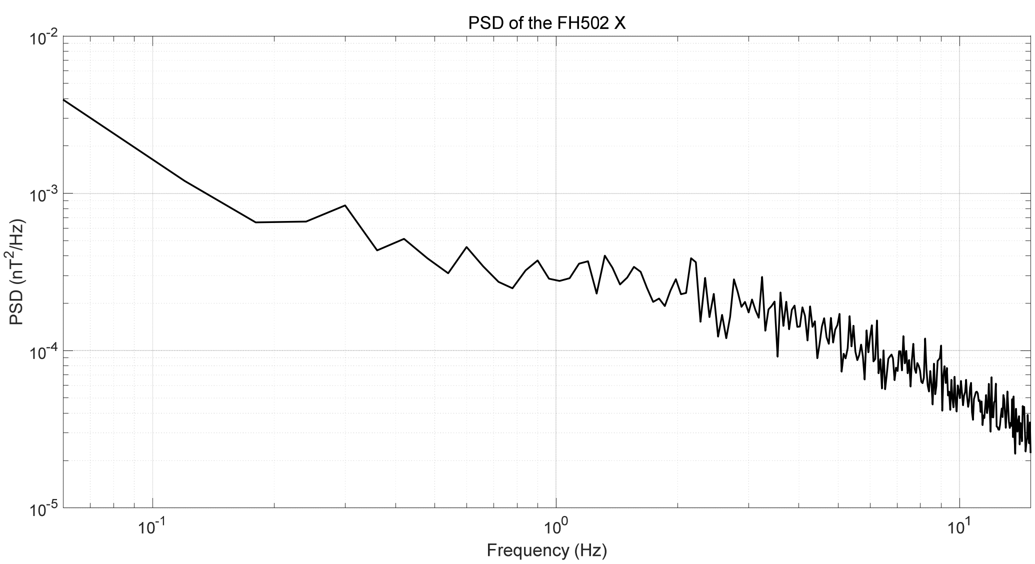

Figure 11. Noise PSD of FGMA X-component

4.5 Temperature drift test

In GEO orbit, solar illumination and Earth shadow alternate in a one-day cycle. So, the temperature of the sensor changes in 24 hours, which is the main source affecting the measurements. The sensor has passive thermal protection, according to the estimated temperature range of ±100℃. The temperature of the electronics box is relatively stable inside the satellite, and the influence of the electronics temperature drift on the measurement can be ignored for a signal processing system adopting a low-temperature drift feedback resistance.

The temperature calibration test was carried out in the laboratory in Yichang. The temperature test cycle is 24 hours, simulating the process of in-orbit heating and cooling. Each sensor had a two cycles test. Figure 12(a) below shows the temperature drift of the sensor offset. The temperature drift of the offset for a fluxgate sensor in a wide temperature range is neither linear nor monotonous. The offset temperature drift curve can be reproduced in the same process of heating and cooling, even with some details. The gain temperature drift is mainly determined by the thermal expansion of the coil materials and structure. It has good linearity and the change is smooth. From the curves of figure 12(b), it can be seen that the drift rate of offset with temperature is less than 0.1nT/℃ and the drift rate of gain with temperature is less than 50 ppm.

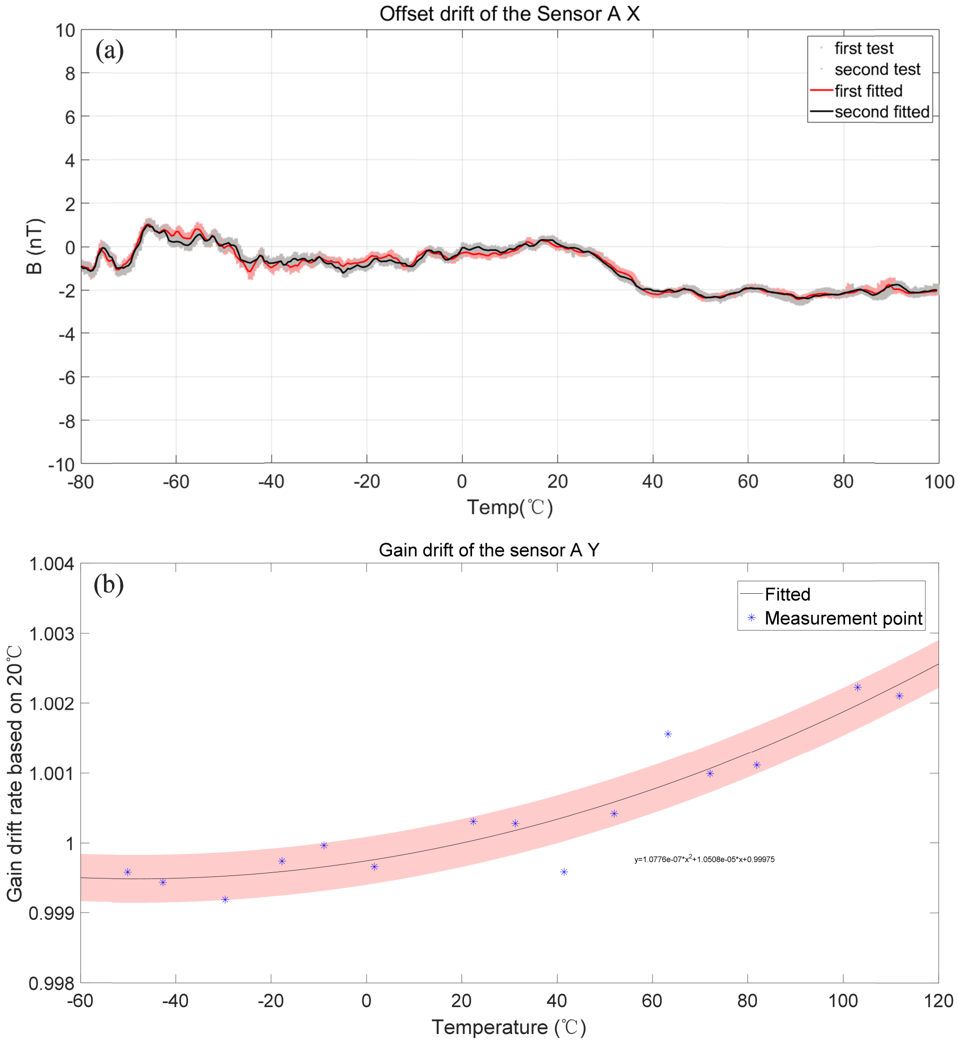

Figure 12. Temperature drift. (a) and (b) show the drift of offset and gain with the temperature of the sensor

4.6 Summary of the ground calibration

Through the ground calibration test, the FGM performance can be confirmed, as shown in Table 1.

Table 1. FGM Performance

Measurement range	±600nT, ±65000nT
Linearity	≤0.04%
Frequency bandwidth	DC～7Hz
Noise	$3\times10^{-4}nT^2/Hz$@1Hz
Orthogonality	≤0.01°
Offset temperature stability	≤0.1nT/℃
Gain temperature stability	≤50ppm

5. In-orbit preliminary results

The three fluxgate sensors are installed near the top of the 6-meter boom on the FY-4B satellite. The influence of satellite remanent magnetism on the sensors has been greatly attenuated, and the static and dynamic interferences from the satellite can be effectively eliminated by the comparative analysis of the three sensors observation. The satellite rotates 180° around the Z axis near the spring and autumn equinoxes, while the X and Y components of the fluxgate sensor also rotate 180° with the satellite. This opportunity can be used to calibrate the Offset of the X and Y components. The calibration of the Z component offset is achieved by observation of the Alfven wave events. Based on the known Offset of the X and Y components, the Z component offset can be calculated according to the Davis-smith equation (Leinweber et al., 2008).

To verify the calibration results, the magnetic field data of FY-4B and GOES-16 satellites were compared in two 7-day periods before and after the rotating attitude of the satellite. FY-4B is located in GEO orbit at 123.4°E, and GOES-16 is located in GEO orbit at 75.2°W (Loto'aniu et al., 2019). The longitudinal difference between the two satellites is about 198°, and the magnetic fields observed by them are very different. For the comparison of two satellite observations, the T89 model is used as a reference, which is an empirical Earth's magnetospheric magnetic field (Tsyganenko, 1989). The model together with the IGRF model can reflect the distribution of the magnetic field within the magnetosphere. From Figure.13, T89 predictions (calculated by the Kp index from Matzka et al. (2021)) are generally consistent with the GOES-16 observations and can be used to evaluate the FY-4B observations. The comparison between the observations of FY-4B before and after the satellite rotation and the model is consistent, which indicates that the offset calibration is effective. The trend of magnetic field variation observed by FY-4B is consistent with the model, which indicates that FY-4B can correctly reflect the magnetic field variation in GEO orbit, just like the GOES-16 satellite.

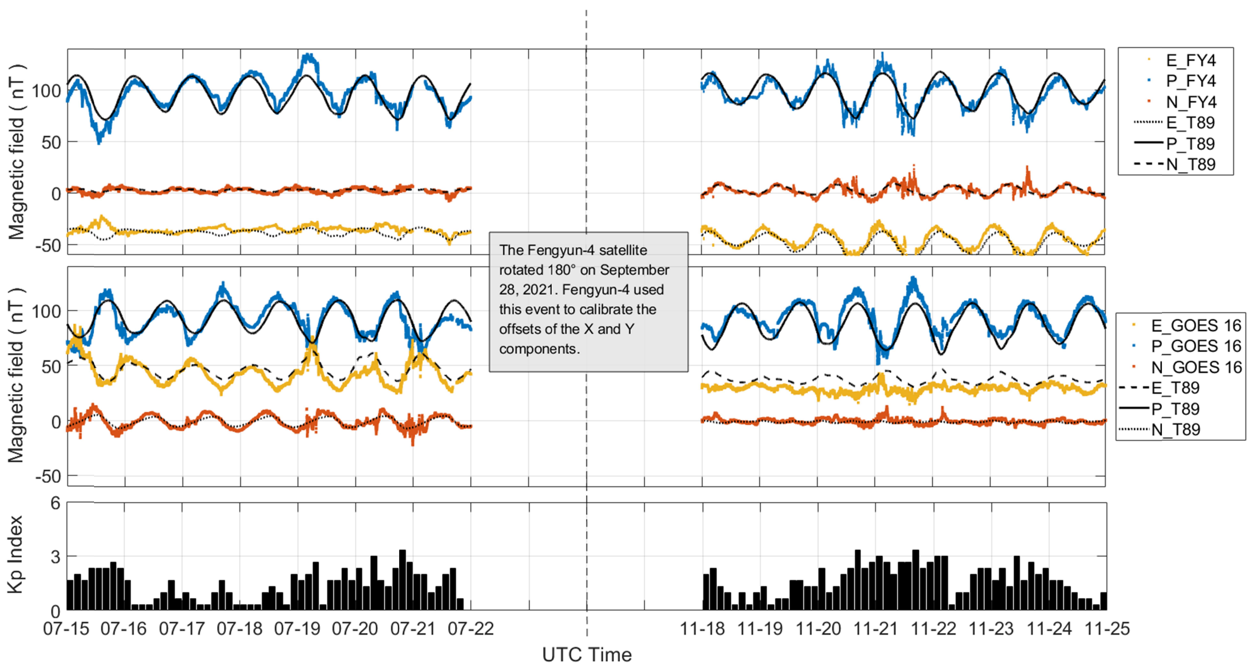

Figure 13. Comparison of magnetic field data from FY-4B and GOES-16 satellites with the T89 model, within two periods before and after September 28, respectively. The offset of the X and Y components of the magnetic field was calibrated during the satellite rotation maneuver on September 28.

A stronger magnetic storm event occurred on November 4, 2021, and was observed by the FY-4B satellite, GOES-16 satellite, and geomagnetic stations. The CME reached Earth on November 3, 2021, at ~20:00 UTC. According to the DST index(Kyoto doi:10.17593/14515-74000), the magnetic storm entered the initial phase. According to the solar wind dynamic pressure, there were two magnetopause compression processes in the initial phase. The main phase began at about 04:00 UTC and peaks at 10:00 UTC the next day with a DST index of -100 nT. During this process, the FY-4B satellite moved from the night side of the dawn terminator (4:00 local time) to the dusk (18:00 local time); the GOES-16 satellite moved from the day side of the dusk terminator (15:00 local time) to the night-side, and finally approached the dawn terminator (5:00 local time). Figure 14 shows the relative positions of the two satellites. Two geomagnetic stations, BMT (40.3°N, 116.2°E) in Beijing and HUA (12.1°S, 75.3°W) in Peru, are close to the longitudes of FY-4B and GOES16 satellites, respectively (Gjerloev, 2012). Figure 15 shows the observations from November 3 to 6 including the magnetic storm. During the 8 hours of the initial phase, FY-4B and GOES-16 satellites observed two obvious magnetic field enhancement processes, the first time GOES-16 (dayside) had an obvious enhancement of about 50nT in the P component, while the magnetic field disturbances of FY-4B (night side) appear in the 3 components. The second time FY-4B (dayside) had an enhancement of about 60 nT in the P component and the GOES-16 satellite (night side) magnetic field disturbances in all three components. When the magnetic storm then enters the main phase, a large number of charged particles are injected into the inner magnetosphere, gradually forming a ring current, which was first seen by GOES-16 located at midnight. FY-4B moved from near the subsolar point to dusk and flew over the region of the ring current growth on the dusk side, thus observing the larger magnetic field generated by the ring current. The disturbed earthward magnetic field was observed on the FY-4B satellite, indicating that the ring current is already very close to the GEO orbit, considering that FY-4B is located south of the magnetic equator. Meanwhile, the GOES-16 satellite flew from midnight to the dawn terminator, observing the magnetic field disturbance earlier than FY-4B, and thereafter magnetic field was significantly less disturbed than that observed by the FY-4B satellite, due to the weaker ring current on the dawn side. Similarly, the magnetic field perturbation observed by HUA on the ground is also significantly weaker than that observed by BMT. The evolution of the ring current in this magnetic storm is consistent with the model description (e.g., Fok et al., 2001).

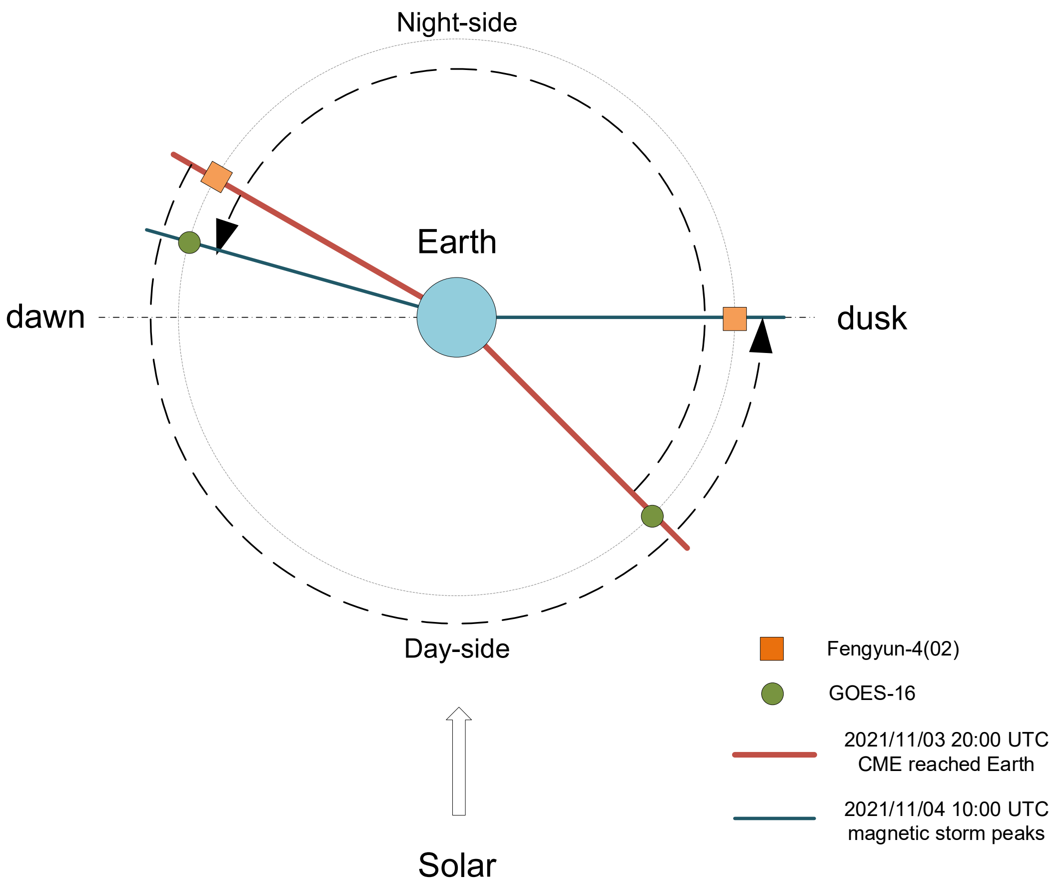

Figure 14. The location of FY-4B and GOES-16 satellites in GEO orbit during the magnetic storm

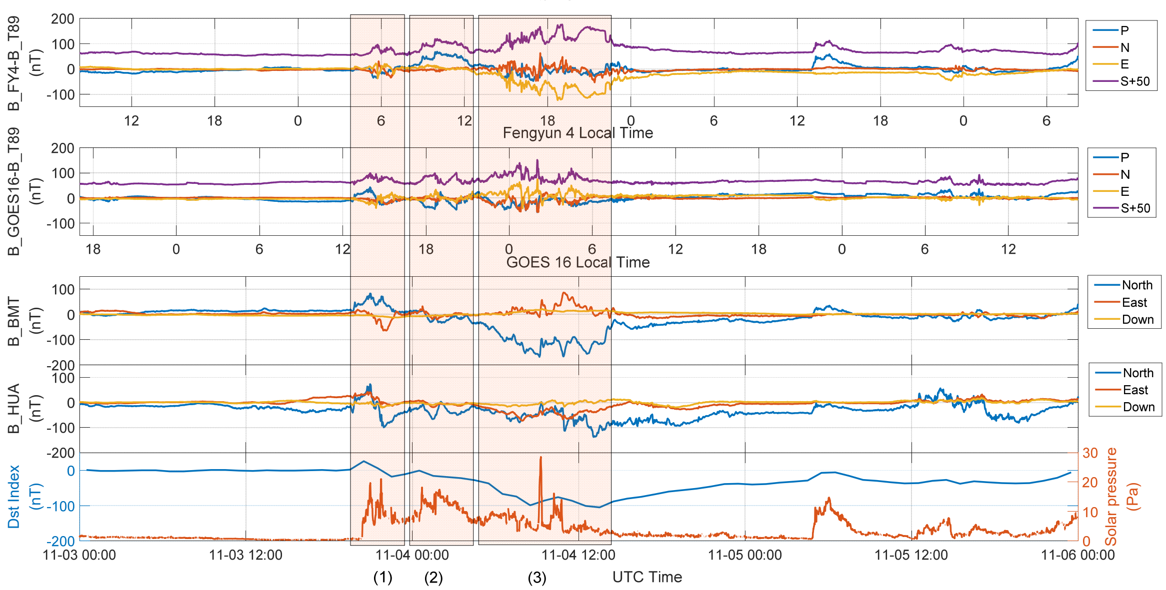

Figure 15. Observations of the magnetic field during the magnetic storm on November 4, 2021. The highlighted interval (1) is the first magnetopause compression in the initial phase. Interval (2) is the second magnetopause compression in the initial phase. Interval (3) is the main phase of the magnetic storm

6 Conclusions

The paper introduces the development, testing, and calibration of the FY-4B digital fluxgate magnetometer. This payload achieves 20-bit digital resolution and 30Hz sampling in a range of ±600nT, and the noise level is lower than 3×10^{-4} nT^2/Hz @1Hz. The ground tests confirm FGM performances meet the requirements of the FY-4 mission. After the in-orbit calibration, the magnetic field observation of the FY-4B satellite is consistent with the GOES-16 satellite observation and prediction by the magnetospheric magnetic field model. As demonstrated by the observation in a typical magnetic storm, the FY-4B satellite magnetometer has the capability for long-term magnetic field monitoring in the GEO orbit.

Acknowledgments

This work was supported by the National Key R&D Program of China (2021YFA0718600), and the National Natural Science Foundation of China (41931073). We gratefully acknowledge the SuperMAG collaborators (https://supermag.jhuapl.edu/info/?page=acknowledgement)

Data Availability Statement

The magnetic field data of FY-4B used in this paper is provided by the China National Satellite Meteorological Center and can be obtained at http://satellite.nsmc.org.cn/. Full access to the data requires an application after real-name registration. Geomagnetic station data can be accessed at the SuperMag website. The geomagnetic indices used in this study can be found at https://doi.org/10.5880/Kp.0001 and http://wdc.kugi.kyoto-u.ac.jp/wdc/Sec3.html for Kp and Dst respectively. And the solar wind dynamic pressure is available at http://omniweb.gsfc.nasa.gov.

References

Baumjohann, W., Matsuoka, A., Magnes, W., Glassmeier, K. H., Nakamura, R., & Al, E. (2010). Magnetic field investigation of Mercury's magnetosphere and the inner heliosphere by MMO/MGF. *Planetary & Space Science, 58*(1-2), 279-286. https://doi.org/10.1016/j.pss.2008.05.019

Cheng, B. J., Zhou, B., Werner, M., Roland, L., & Andreas, P. (2018). High precision magnetometer for geomagnetic exploration onboard the China Seismo-Electromagnetic Satellite. *Science China: Technological Sciences, 61*(5), 659-668. https://doi.org/10.1007/s11431-018-9247-6

Erik, B. P., Fritz, P., Jan, R. P., Merayo, J. M. G., Peter, B., & Nielsen, O. V. (1999). Digital fluxgate magnetometer for the Astrid-2 satellite. *Measurement Science and Technology, 10*(11), N124. https://dx.doi.org/10.1088/0957-0233/10/11/402

Fok, M.-C., Wolf R. A., Spiro R. W., and Moore T. E. (2001). A comprehensive computational model of the Earth's ring current, *Journal of Geophysical Research*, 106, 8417-8424. https://doi.org/10.1029/2000JA000235

Glassmeier, K. H., Auster, H. U., Heyner, D., Okrafka, K., Carr, C., Berghofer, G., et al. (2010). The fluxgate magnetometer of the BepiColombo Mercury Planetary Orbiter. *Planetary and Space Science, 58*(1), 287-299. https://doi.org/10.1016/j.pss.2008.06.018

Gjerloev, J. W. (2012). The SuperMAG data processing technique. Journal of Geophysical *Research: Space Physics, 117*(A9). https://doi.org/10.1029/2012JA017683

Leinweber, H. K., Russell, C. T., Torkar, K., Zhang, T. L., & Angelopoulos, V. (2008). An advanced approach to finding magnetometer zero levels in the interplanetary magnetic field. *Measurement Science and Technology, 19*(5), 055-104. https://dx.doi.org/10.1088/0957-0233/19/5/055104

Loto'aniu, T. M., Redmon, R. J., Califf, S., Singer, H. J., Rowland, W., Macintyre, S., et al. (2019). The GOES-16 Spacecraft Science Magnetometer. *Space Science Reviews, 215*(4), 32. https://doi.org/10.1007/s11214-019-0600-3

Matzka, J., Stolle, C., Yamazaki, Y., Bronkalla, O. and Morschhauser, A. (2021). The geomagnetic Kp index and derived indices of geomagnetic activity. *Space Weather, 19*(5), e2020SW002641.https://doi.org/10.1029/2020SW002641

Tsyganenko, N. A. (1989). A magnetospheric magnetic field model with a warped tail current sheet. *Planetary and Space Science, 37*, 5-20. https://ui.adsabs.harvard.edu/abs/1989P&SS...37....5T

Yang, J., Zhang, Z., Wei, C., Lu, F., & Guo, Q. (2017). Introducing the New Generation of Chinese Geostationary weather Satellites, Fengyun-4. *Bulletin of the American Meteorological Society, 98*(8),1637-1658. https://doi.org/10.1175/BAMS-D-16-0065.1

Zhang, T. L., Berghofer, G., Magnes, W., Delva, M., & Richter, I. (2007). MAG: The Fluxgate Magnetometer of Venus Express. ESA special publication. SP 1295, 1-10.

Zhou, B., Zhao, H., Wang, J., Chen, S., & Jingxuan, Z. (2009). Martian Space Environment Magnetic Field Investigation---High Accuracy Magnetometer. *Chinese Journal of Space Science*. *29*(5), 467-474. https:// doi: 10.11728/cjss2009.05.467

Zhou, B., Yang, Y., Zhang, Y., Gou. X., et al. (2018). Magnetic field data processing methods of the ChinaSeismo-Electromagnetic Satellite. *Earth and Planetary Physics, 2*(6), *455–461.* https://doi.org/10.26464/epp2018043